

Activation cross sections of proton induced nuclear reactions on palladium up to 80 MeV

F. Tárkányi^a, F. Ditrói^{a,*}, S. Takács^a, J. Csikai^a, A. Hermanne^b, S. Uddin^d, M. Baba^d

^a*Institute for Nuclear Research, Hungarian Academy of Sciences (ATOMKI), Debrecen, Hungary*

^b*Cyclotron Laboratory, Vrije Universiteit Brussel (VUB), Brussels, Belgium*

^c*Institute of Physics and Power Engineering (IPPE), Obninsk, Russia*

^d*Cyclotron Radioisotope Center (CYRIC), Tohoku University, Sendai, Japan*

Abstract

Activation cross sections of proton induced nuclear reactions on palladium were measured up to 80 MeV by using the stacked foil irradiation technique and gamma ray spectrometry. The beam intensity, the incident energy and the energy degradation were controlled by a method based on flux constancy via normalization to the excitation functions of monitor reactions measured in parallel. Excitation functions for direct and cumulative cross-sections were measured for the production of $^{104m,104g,105g,106m,110m}\text{Ag}$, $^{100,101}\text{Pd}$, $^{99m,99g,100,101m,101g,102m,102g,105}\text{Rh}$ and $^{103,97}\text{Ru}$ radioisotopes. The cross section data were compared with the theoretical predictions of TENDL-2014 and -2015 libraries. For practical applications thick target yields were derived from the measured excitation functions. Application in the field of medical radionuclide production is shortly discussed.

Keywords: proton irradiation, palladium target, stacked foil technique, cross sections, production yields

1. Introduction

Excitation functions of proton induced nuclear reactions on palladium are important in many applications including medical radioisotope production, determination of elemental impurities by activation analysis, development of low activation materials and others (Khandaker et al., 2010; Skakun and Rauscher, 2007). At present only very few experimental data exist in the literature for light ion induced nuclear reactions on this material. The present investigations were initiated with the aim to investigate the production possibilities of some medically related radioisotopes (^{104}Ag , ^{101}Rh , ^{103}Pd) and to produce reliable activation curves for thin layer activation (^{105}Ag). We already reported the activation cross sections of proton, deuteron, ^3He and alpha-particle induced reactions on Pd for these three radionuclides (Ditrói et al., 2012, 2007; Hermanne et al., 2004a, 2005; IAEA-NDS, 2010; Tárkányi et al., 2009). Regarding the proton activation data, our earlier experiments were performed in 2002-2004 and at that moment only a few earlier low energy work on (p,n) reactions were found in the literature (Batii et al., 1988;

Hu et al., 1998; Johnson et al., 1979; Kormali et al., 1976; Zarubin and Sergeev, 1989). Our results obtained in that period for some medically relevant radionuclides were published during 2004-2007. Since then a detailed study of Pd activation by protons up to 40 MeV was published by (Khandaker et al., 2010), low energy data for formation of ^{105}Ag were published by (Dillmann, 2006; Dillmann et al., 2011). As we had the opportunity to extend the experimental cross sections for all reaction products formed in proton irradiation on Pd up to 80 MeV, we decided to report our new results complemented with all our unpublished data.

2. Experimental

The irradiations were carried out at the external beam lines of the AVF cyclotron at the Tohoku University, Japan at 80 MeV and the CGR 560 cyclotron at the Vrije Universiteit Brussels at 37.3, 28.5 and 15.9 MeV irradiation energies. High purity Pd foils were stacked with Al, Cu and Ti monitor foils and irradiated for 0.1–1.0 hours at 200 nA nominal beam intensity. All foils were purchased from Goodfellow ©, England and were at least 99.7% pure. The beam intensity, the incident energy and the energy degradation were con-

*Corresponding author: ditroi@atomki.hu

trolled by a method based on flux constancy via normalization (including fitting) to the excitation functions of $^{27}\text{Al}(p,x)^{22,24}\text{Na}$ and $^{nat}\text{Cu}(p,x)^{56,58}\text{Co}$, $^{62,65}\text{Zn}$ and $^{nat}\text{Ti}(p,x)^{48}\text{V}$ monitor reactions re-measured in parallel over the whole investigated energy range (see Table 1) (Tárkányi et al., 2001). Measurement of the gamma-ray spectra of the activated foils was carried out without chemical separation. The measurements were started from a few hours up to several weeks after EOB.

The beam currents were deduced from the monitor reactions, the number of the target nuclei from the precise mass and surface determination of the target foils. The calculated (by using home-made code based on (Andersen and Ziegler, 1977) energy degradation of the incident beam was checked and corrected on the basis of the monitor reactions. For calculation of the activity of the produced radioisotopes the decay data (Table 3) were taken from (NuDat, 2014).

The uncertainties of the cross-sections were estimated from the linearly contributing processes supposing equal sensitivities. The total resulting errors were between 8 % and 13 %. In the estimation of the uncertainty of the medium proton energy in each target foil in addition to the well-known beam energy broadening, the cumulative propagation of the uncertainty in the energy of the incident beam and in the foil thickness were taken into account.

The experimental and data evaluation details for our different irradiations are collected in Table 1 and Table 2, the used decay data and the Q-values of the contributing reactions in Table 3.

3. Results and discussion

3.1. Cross sections

The measured cross sections for the production of $^{103,104m,104g,105g,106m,110m}\text{Ag}$, $^{100,101}\text{Pd}$, $^{99m,100m,100,101m,101g,102m,102g,105}\text{Rh}$ and $^{103,97}\text{Ru}$ are shown in Table 4-5 and Figures 1-18. The figures also show the earlier literature experimental results and the theoretical results calculated with the TALYS code (Koning and Rochman, 2012) as listed in the TENDL-2014 (Koning et al., 2014) and 2015 (Koning et al., 2015) on-line libraries. For total production cross sections also the ALICE-IPPE (Dityuk et al., 1998) results are shown, taken from the MENDL-2P library (Shubin et al., 1998) where these data are available for some assessed activation products.

Due to the experimental circumstances (stacked foil technique, large number of simultaneously irradiated

target, high radiation dose rate at EOB, limited detector capacity, limited available time for spectra measurements) no cross section data were obtained for some short-lived activation products. In cases of low energy unresolved gamma-rays, small effective cross section or low abundance some characteristic γ -lines could not be identified in the measured spectra. If this happens to be the only γ -line of an activation product, unfortunately no cross-sections could be obtained.

The results are discussed separately for each reaction product. Naturally occurring palladium is composed of 6 stable isotopes (^{102}Pd : 1.02 %, ^{104}Pd : 11.14 %, ^{105}Pd : 22.38 %, ^{106}Pd : 27.33 %, ^{108}Pd : 26.46 % and ^{110}Pd : 11.72 %) (Berglund and Wieser, 2011). The relevant contributing reactions are collected in Table. 3.

The silver isotopes are produced only through (p,xn) reactions, the palladium isotopes directly via (p,pxn) reactions and through the EC- β^+ decay of silver and β^- decay of isobaric rhodium radio-parents, the rhodium radioisotopes are produced through direct (p,2pxn) reactions (including clustered particle emissions) and EC- β^+ decay of simultaneously produced isobaric palladium radio-products.

The results of our different irradiation series show only moderate agreement overall. In case of low statistics, the disagreement is more or less understandable, but the systematic disagreements, mostly between values obtained from irradiations and measurements performed at another location, are more difficult to explain. The different experimental circumstances can result in deviations of the used beam intensities often due to different detector efficiencies that cannot be cross-checked between the measuring sites. Also monitors and targets were often measured at different detector-target distances, which could result in systematic offsets. In many cases automatic peak fitting was used with different commercial analyzing software, which could cause systematic errors. As in most cases no earlier experimental data were available, we thought it worthwhile to show all experimental results from our multiple datasets, even if in the name of scientific honesty, we recognize that some discrepancies exist.

3.1.1. Radioisotopes of silver

3.1.1.1 $^{nat}\text{Pd}(p,xn)^{110m}\text{Ag}$ reaction

The radionuclide ^{110}Ag has two long-lived states. The high spin isomeric state ($I^\pi = 6^+$, $T_{1/2} = 249.8$ d) decays with β^- (98.67 %) to ^{110}Cd and with IT (1.33%) to the short-lived ground state ($I^\pi = 1^+$, $T_{1/2} = 24.6$ s). Only the $^{110}\text{Pd}(p,n)$ reaction is contributing. The mea-

Table 1: Main parameters of the experiments and the methods of data evaluations

Experiment							
Reaction	<i>nat</i> Pd(p,x)						
Method	Stacked foil						
Irradiation(year)	2002	2002	2003	2004	2002	2002	2002
Identification	S2002-1	S2002-2	S2003	S2004	V1	V2	V3
Target stack and thicknesses (μm)	Cu 54.4 Pd 12 Al 97.8 Pt 9.29 Al 97.8 Ta 8.63 block repeated 9 times	Cu 54.4 Ta 209.7 Pd 9.5 Al 97.8 Fe 25.4 block repeated 10 times	Cu 54.4 Al 1000 Pd 12.1 Cd 15 Al 1000 block repeated 10 times	Cu 54.4 Mo 49.6 Y 110.4 Pd 12.5 Ag 303 Cd 15 Al 495 or 1000 block repeated 10 times	Cu 23.92 Ti 12.02 Pd 7.99 repeated 9 times	Ni 23.97 Pd 7.99 Ti 30.58 Ta 8.63 repeated 10 times	Ni 23.97 Pd 7.99 Cu 23.92 Al 100 Ti 30.58 Pd 7.99 Ta 8.63 Al 100 repeated 10 times
Number of Pd target foils	9	10	10	10	9	10	10
Accelerator	K110 MeV cyclotron CYRIC, Sendai	K110 MeV cyclotron CYRIC, Sendai	K110 MeV cyclotron CYRIC, Sendai	K110 MeV cyclotron CYRIC, Sendai	CGR-560 cyclotron VUB Brussels	CGR-560 cyclotron VUB Brussels	CGR-560 cyclotron VUB Brussels
Primary energy (MeV)	70(±0.3)	70(±0.3)	70(±0.3)	80(±0.3)	15.9(±0.2)	28.5(±0.2)	37.3(±0.2)
Energy range covered (for Pd) (MeV)	69.5-28.9	64.4-42.8	67.7-34.1	79.9-37.4	15.8-6.7	28.2-15.9	37.0-20.0
Irradiation time (min)	60	60	6.4	71	30	30	30
Beam current (nA)	90	100	160	49.6	170.4	183.7	175.5
Monitor reaction, [recommended values]	$^{27}\text{Al}(p,x)^{22,24}\text{Na}$ $^{nat}\text{Cu}(p,x)^{62,65}\text{Zn}$	$^{27}\text{Al}(p,x)^{22,24}\text{Na}$ $^{nat}\text{Cu}(p,x)^{62,65}\text{Zn}$	$^{27}\text{Al}(p,x)^{22,24}\text{Na}$ $^{nat}\text{Cu}(p,x)^{62,65}\text{Zn}$	$^{27}\text{Al}(p,x)^{22,24}\text{Na}$ $^{nat}\text{Cu}(p,x)^{62,65}\text{Zn}$	$^{nat}\text{Cu}(p,x)^{62,65}\text{Zn}$ $^{nat}\text{Ti}(p,x)^{48}\text{V}$	$^{nat}\text{Cu}(p,x)^{62,65}\text{Zn}$ $^{nat}\text{Ti}(p,x)^{48}\text{V}$	$^{nat}\text{Cu}(p,x)^{62,65}\text{Zn}$ $^{nat}\text{Ti}(p,x)^{48}\text{V}$
Detector	HPGe	HPGe	HPGe	HPGe	HPGe	HPGe	HPGe
γ-spectra measurements	3 series	3 series	2 series	2 series	3 series	3 series	3 series
Cooling times (h)	55.1-57.1 87.0-102.9 562-658	37.0-39.2 105.3-109.4 920-993	0.7-1.4 34.1-67.7	20.7-23.8 74.1-98.9	0.7-2.3 27.0-30.4 31.8-150.1	0.7-2.7 40.1-49.8 49.4-194.8	1.7-5.0 24.8-31.9 341.4-456.3
Earlier published (from these experiments) (Ditrói et al., 2007; Hermanne et al., 2004b; Tárkányi et al., 2009)	^{105}Ag ^{106m}Ag ^{100}Pd ^{101m}Rh	^{105}Ag ^{106m}Ag ^{100}Pd ^{101m}Rh	^{103}Ag , ^{103}Pd		^{103}Ag ^{105}Ag ^{106m}Ag ^{104g}Ag	^{103}Ag ^{105}Ag ^{106m}Ag ^{104g}Ag	^{103}Ag ^{105}Ag ^{106m}Ag ^{110m}Ag ^{104g}Ag

sured and calculated cross-sections for ^{110m}Ag production are shown in Fig. 1. All series of measurements are compatible with the published values below 10 MeV (Batii et al., 1988; Dillmann et al., 2011). The TENDL-2015 predictions describe well the region from threshold to maximum but overestimate above 12 MeV. The previous TENDL-2014 gives better prediction around the maximum.

3.1.1.2 $^{nat}\text{Pd}(p,xn)^{106m}\text{Ag}$ reaction

The production cross-sections for the long-lived isomeric state ($I^\pi = 6^+$, $T_{1/2} = 8.28$ d, $\epsilon: 100\%$) were measured and are shown in Fig. 2. Our new values agree with the earlier experimental results of (Khandaker et al., 2010) above 35 MeV, and agree well with the TENDL predictions. Also the agreement with the data of (Ditrói et al., 2007) is good while the few low energy point of (Dillmann et al., 2011) are compatible with the data of (Khandaker et al., 2010).

3.1.1.3 $^{nat}\text{Pd}(p,xn)^{105m,g}\text{Ag}$ reaction

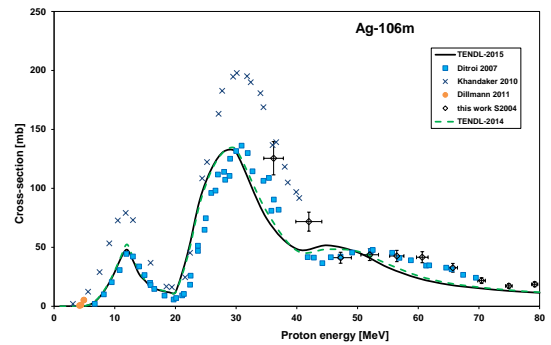
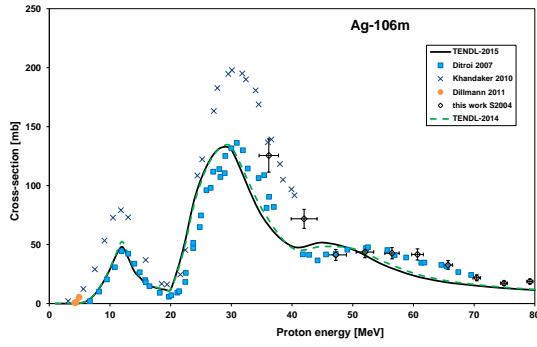
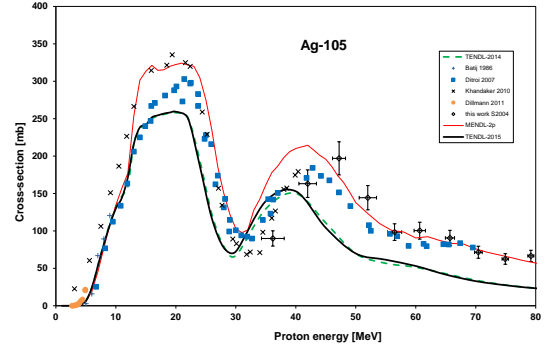
Figure 1: Experimental and theoretical cross section values for proton induced ^{110m}Ag production on natural palladium

Table 2: Methods of data evaluation

Data evaluation	
Method	Preliminary study of earlier experimental data and theoretical predictions
Gamma spectra evaluation	Genie 2000, Forgamma (Canberra, 2000; Székely, 1985), automatic and manual controlled peak fitting
Determination of beam intensity	Faraday cup (preliminary), Fitted monitor reaction (final) (Tárkányi et al., 1991) (see Table 1)
Decay data	NUDAT 2.6 (Kinsey et al., 1997; NuDat, 2014) Toi Lund database (Chu et al., 1999) for data missing in NUDAT (BNL, 2015)
Reaction Q-values	Q-value calculator (Pritychenko and Sonzogni, 2003)
Determination of beam energy	Andersen (Andersen and Ziegler, 1977)(calculated, preliminary), Fitted monitor reactions (final)
Uncertainty of energy	Cumulative effects of possible uncertainties (primary energy, foil thickness and uniformity, energy straggling)
Cross sections	Elemental cross section
Uncertainty of cross sections	Sum in quadrature of all individual contribution (International-Bureau-of-Weights-and-Measures, 1993): (uncertainty on beam current %, target thickness %, detector efficiency calibration %, γ -ray abundance and statistical uncertainty on count rates %) The contributions of the uncertainties of non-linear parameters were neglected (cooling times, half-life).
Yield	Calculated from cross sections Physical yield (Bonardi, 1987)
Theory	TALYS (TENDL-2014 and 2015) (Koning et al., 2014)

Figure 2: Experimental and theoretical cross section values for proton induced ^{106m}Ag production on natural palladiumFigure 3: Experimental and theoretical cross section values for proton induced ^{105}Ag (cumulative) production on natural palladium

The radionuclide ^{105}Ag has also two long-lived states. The shorter-lived isomeric state ($I^\pi = 7/2^+$, $T_{1/2} = 7.7$ min) decays with 99.66 % by internal transition to the ground state ($I^\pi = 1/2^-$, $T_{1/2} = 41.3$ d). The cumulative production cross sections for the ground state, after complete decay of the meta-stable state, were measured. The values are compared with the earlier results and with model calculation in Fig. 3. The agreement with the experimental data in the literature is acceptable both in shape and in the absolute values within 10 %. The high energy part of the TENDL-2015 data seems to be shifted to lower energies.

3.1.1.4 $^{nat}\text{Pd}(p,xn)^{104m}\text{Ag}$ and $^{nat}\text{Pd}(p,xn)^{104g}\text{Ag}$ reactions

The radionuclide ^{104}Ag has two states. The shorter-lived isomeric state ($I^\pi = 2^+$, $T_{1/2} = 33.5$ min) decays with 36.93 % EC + 63 % β^+ to ^{104}Pd and by 0.07 % internal transition to the ground state ($I^\pi = 5^+$, $T_{1/2} = 69.2$

min). We could deduce independent production cross sections for both states after small corrections ($< 5\%$) for internal transitions. The experimental and theoretical cross-sections are shown in Figs. 4-5. The agreement with the theory and the earlier experimental data is acceptable for the formation of ^{104m}Ag although our data V2 do not represent properly the dip around 25 MeV and the TENDL-2015 values are shifted downward in energy. For formation of ^{104g}Ag all datasets are agreeing well and show the contributions of the different stable target isotopes, except for the data above 13 MeV of (Kormali et al., 1976). For ^{104m}Ag our new data do not agree with the earlier data sets in the overlapping energy region (only 1 data point), and those are even not compatible with each other. Because of the observable difference between TENDL-2014 and TENDL-2015, both curves are presented in Figs. 4 and 5.

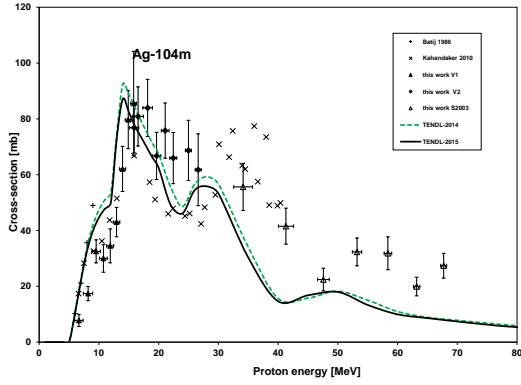


Figure 4: Experimental and theoretical cross sections for proton induced ^{104m}Ag production on natural palladium

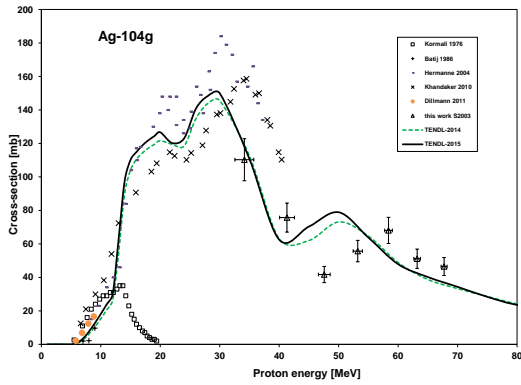


Figure 5: Experimental and theoretical cross sections for proton induced ^{104g}Ag production on natural palladium

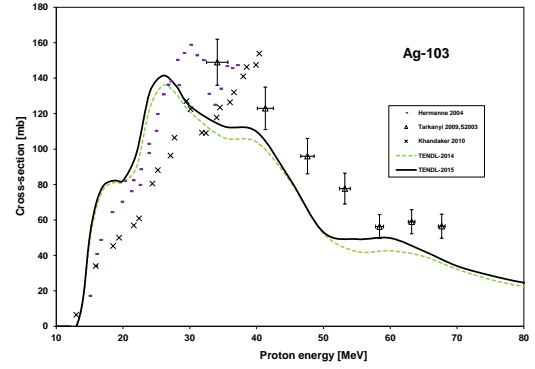


Figure 6: Experimental and theoretical cross sections for proton induced ^{103}Ag production on natural palladium

3.1.1.5 $^{nat}\text{Pd}(p,xn)^{103g}\text{Ag}$ reaction

The experimental and theoretical activation cross-section data for ^{103}Ag ($I^\pi = 7/2^+$, $T_{1/2} = 65.7$ min, ϵ : 100 %) are shown in Fig. 6. The production cross section of the ground state were deduced from spectra measured after complete decay of short-lived metastable state ($I^\pi = 1/2^-$, $T_{1/2} = 5.7$ s, IT: 100 %) and are hence cumulative. These particular data were already published in a special paper on ^{103}Pd production (Tárkányi et al., 2009). The agreement with (Hermanne et al., 2004a) is good while the results of (Khandaker et al., 2010) are somewhat lower and are not decreasing above 40 MeV. The both previous data sets are not compatible with each other. The TENDL values show clearly the multiple contributions of five stable Pd isotopes but seem to be shifted by 3-4 MeV.

3.1.2. Radioisotopes of palladium

3.1.2.1 $^{nat}\text{Pd}(p,x)^{101}\text{Pd}$ reaction

The ^{101}Pd ($I^\pi = 5/2^+$, $T_{1/2} = 8.47$ h, EC: 92.8%, β^+ : 7.2 %) is produced directly via (p,pxn) reaction and through the decay of the short-lived ^{101}Ag parent ($I^\pi = 9/2^+$, $T_{1/2} = 11.1$ min, EC+ β^+ : 100%). The cumulative measured and calculated cross-sections are shown in Fig. 7. There is a good agreement with the earlier experimental data of (Khandaker et al., 2010) and with the TALYS data in the TENDL-2015 library under 32 and above 55 MeV. An unexpected drop of some points of our V2 data set can be observed. MENDL-2P gives good estimation between 40 and 60 MeV.

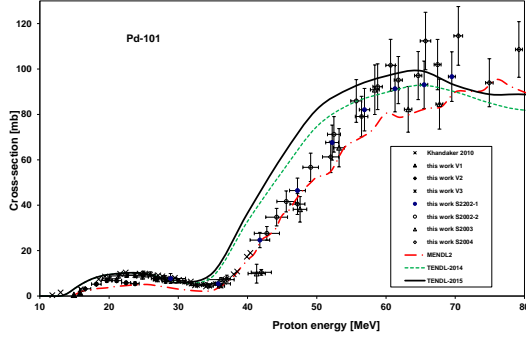


Figure 7: Experimental and theoretical cross sections for proton induced ^{101}Pd production on natural palladium

3.1.2.2 $^{nat}\text{Pd}(p,x)^{100}\text{Pd}$ reaction

The excitation function for production of ^{100}Pd ($I^\pi = 0^+$, $T_{1/2} = 3.63$ d, ϵ : 100 %), after the decay of both isomers of the short-lived $^{100m,g}\text{Ag}$ ($I^\pi = 5^+$, $T_{1/2} = 2.01$ min, EC+ β^+ : 100 % and $I^\pi = 2^+$, $T_{1/2} = 2.24$ min, EC+ β^+ : 100 %) parent nuclei is shown in Fig. 8. According to the figure the TENDL-2014 underestimates the experimental data. Below 40 MeV the data of (Khandaker et al., 2010) are lower than our values in this energy region. A significant scattering can be observed in our V2 and V3 data sets under 30 MeV, probably because of the bad statistics. A significant improvement is seen in the TENDL-2015 version above 45 MeV. MENDL-2P shows a better trend above 60 MeV.

3.1.3. Radioisotopes of rhodium

3.1.3.1 $^{nat}\text{Pd}(p,x)^{105}\text{Rh}$ reaction

The cumulative excitation functions for production of the ^{105g}Rh ground state ($I^\pi = 7/2^+$, $T_{1/2} = 35.36$ h, β^- : 100 %), measured after complete isomeric decay of the short-lived metastable state ^{105m}Rh ($I^\pi = 1/2^-$, $T_{1/2} = 42.9$ s, IT: 100 %) are shown in Fig. 9. The ^{105g}Rh is produced via (p,2pxn) reactions on higher mass (106-110) stable Pd isotopes. The agreement with (Khandaker et al., 2010) is very good but the theory significantly underestimates the experiment up to 40 MeV (Fig. 9). Our data show strong scattering and slight disagreement with each other above 40 MeV, probably because of the worse statistics, which is also reflected in the error bars. No significant difference was observed between the two TENDL versions.

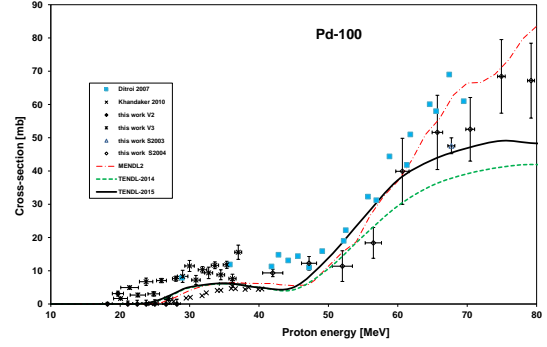


Figure 8: Experimental and theoretical cross sections for proton induced ^{100}Pd (cumulative) production on natural palladium

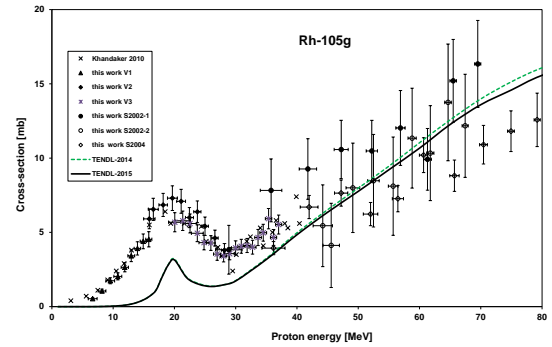


Figure 9: Experimental and theoretical cross sections for proton induced ^{105}Rh production on natural palladium

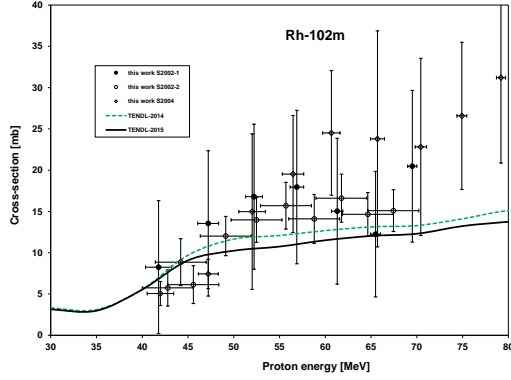


Figure 10: Experimental and theoretical cross sections for proton induced ^{102m}Rh production on natural palladium

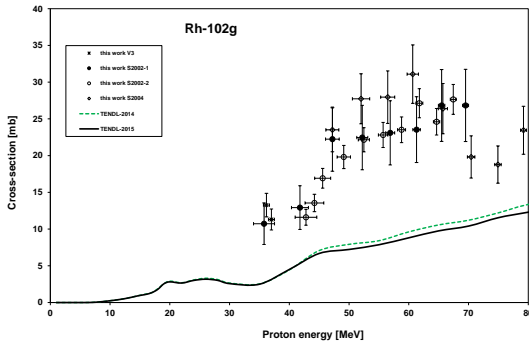


Figure 11: Experimental and theoretical cross sections for proton induced ^{102g}Rh production on natural palladium

3.1.3.2 $^{nat}\text{Pd}(p,x)^{102m}\text{Rh}$ and $^{nat}\text{Pd}(p,x)^{102g}\text{Rh}$ reactions

The radionuclide ^{102}Rh has two long-lived states. The excitation functions for independent production of ^{102m}Rh metastable state ($I^\pi = 0^+$, $T_{1/2} = 3.742$ a, EC: 99.767 %, IT: 0.233 %) and ^{102}Rh ground state ($I^\pi = 1/2^-$, $T_{1/2} = 207.3$ d, EC: 62.3 %, β^+ : 15.7%, β^- 22 %) are shown in Fig. 10 and 11. The data are strongly scattered because of the low statistics, but in average follow the trend of the TENDL curves for the ^{102m}Rh isotope. The ^{102g}Rh results are even more scattered and far above the TENDL-predictions.

3.1.3.3 $^{nat}\text{Pd}(p,x)^{101m}\text{Rh}$ and $^{nat}\text{Pd}(p,x)^{101g}\text{Rh}$ reactions

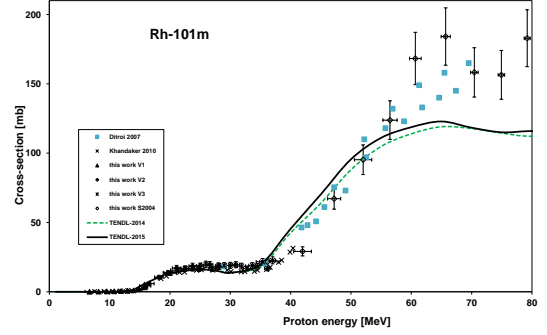


Figure 12: Experimental and theoretical cross sections for proton induced ^{101m}Rh production on natural palladium

Out of the two longer-lived states of ^{101}Rh , the ^{101m}Rh isomeric state ($I^\pi = 9/2^+$, $T_{1/2} = 4.34$ d, IT: 7.2 % EC: 92.8 %) is produced directly through the $^{nat}\text{Pd}(p,2pxn)^{101m}\text{Rh}$ process but is also fed from the mother ^{101}Pd ($T_{1/2} = 8.47$ h).

The cumulative cross sections of the ^{101m}Rh isotope, deduced after complete decay of the ^{101}Pd parent, is shown in Fig. 12. All data sets agree well and the theoretical prediction in TENDL-2015 only diverge above 55 MeV. There is a good agreement with the previous results and also with the TENDL predictions up to 60 MeV, above this energy the TENDL predictions slightly underestimate the experimental results.

The ^{101g}Rh ground state ($I^\pi = 1/2^-$, $T_{1/2} = 3.3$ a, ϵ : 100 %) is produced directly and through the 7.2 % internal decay of the meta-stable state. The cumulative productions cross sections (m1+) obtained from the late spectra are shown in Fig. 13. The data points from our different experiments agree with each other, although the S2004 shows large scattering. The TENDL predictions underestimate the experimental results.

3.1.3.4 $^{nat}\text{Pd}(p,x)^{100g}\text{Rh}$ reaction

The deduced cumulative cross sections of ^{100g}Rh ($I^\pi = 1^-$, $T_{1/2} = 20.8$ h, EC: 96.1 %, β^+ : 3.9 %) (Fig. 14) include the direct production and the production through total decay of the short-lived isomeric state ($I^\pi = 5^+$, $T_{1/2} = 4.6$ min, IT 98.3 %, EC: 1.7 %). The contribution from the decay of ^{100}Pd (3.63 d) was deduced. All experimental data-sets agree well and TENDL shows a larger dip than the experiments in the 40-60 MeV region. The MENDL-2P data represent only the direct

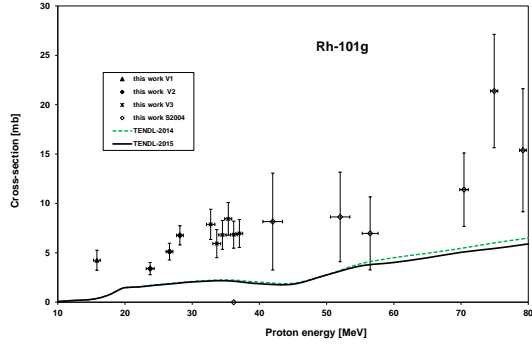


Figure 13: Experimental and theoretical cross sections for proton induced $^{101g}\text{Rh}(m+)$ production on natural palladium

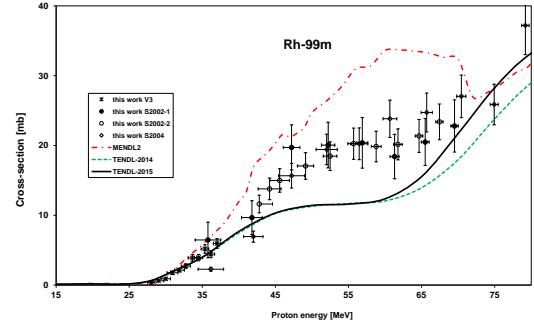


Figure 15: Experimental and theoretical cross sections for proton induced ^{99m}Rh production on natural palladium

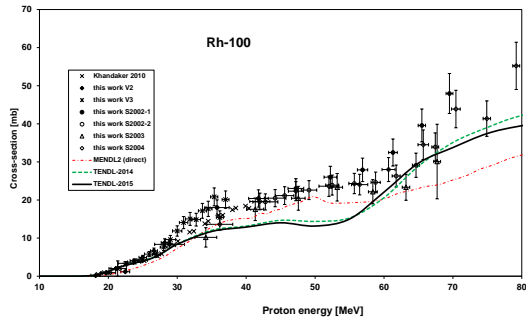


Figure 14: Experimental and theoretical cross sections for proton induced $^{100}\text{Rh}(\text{cumulative})$ production on natural palladium

production, that's why they show a stronger underestimation above 60 MeV.

3.1.3.5 $^{nat}\text{Pd}(p,x)^{99m}\text{Rh}$ and $^{nat}\text{Pd}(p,x)^{99g}\text{Rh}$ reactions

The two long-lived states of ^{99}Rh are decaying independently. They are produced directly and the metastable state ^{99m}Rh is also populated through the decay of short-lived ^{99}Pd parent ($T_{1/2} = 21.4$ min). The excitation function for cumulative production of the ^{99m}Rh metastable state ($I^\pi = 9/2^+$, $T_{1/2} = 4.7$ h, $IT < 0.16$ %, $EC: 92.7$ %, $\beta^+: 7.3$ %), including the 97.4 % decay contribution of ^{99}Pd is shown in Fig. 15. The agreement between our different data sets is acceptable good in the overlapping energy region. The data set V3 had a much better statistic, as seen in the error bars. The TENDL calculations give only good estimation up to 37 MeV, above this

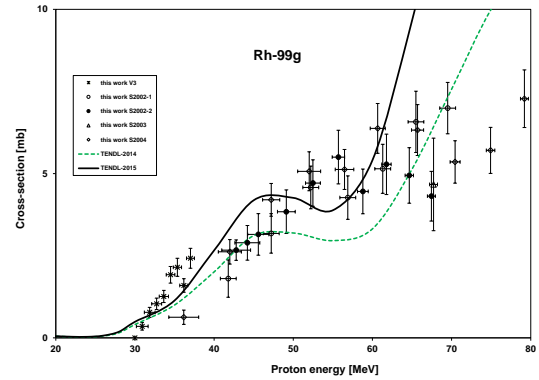


Figure 16: Experimental and theoretical cross sections for proton induced ^{99g}Rh production on natural palladium

energy they underestimate up to 70 MeV. MENDL-2P gives a strange curve, which does not follow the trend of the experiment at all.

The cumulative cross sections of the ^{99g}Rh ground state ($I^\pi = 1/2^-$, $T_{1/2} = 16.1$ d, $EC: 96.4$ %, $\beta^+: 3.6$ %), including 2.6 % decay contribution from ^{99}Pd parent are shown in Fig. 16. There is an acceptable agreement between the different measurements series. The trend and magnitude of the TENDL predictions follow well the experimental results up to 60 MeV, but above this value the new TENDL-2015 gives overestimated results. It is difficult to decide, which TENDL version gives better estimation.

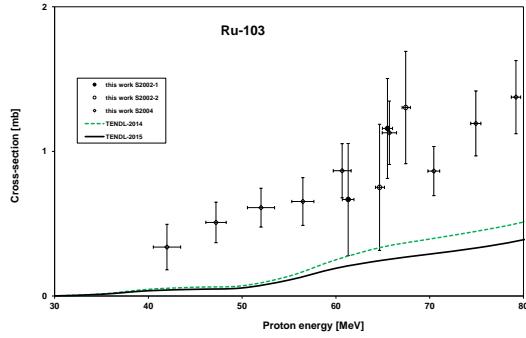


Figure 17: Experimental and theoretical cross sections for the proton induced ^{103}Ru production on natural palladium

3.1.4. Radioisotopes of ruthenium

3.1.4.1 $^{nat}\text{Pd}(p,x)^{103}\text{Ru}$ reaction

The cumulative cross sections of the ^{103}Ru ground state ($I^\pi = 3/2^+$, $T_{1/2} = 39.247$ d, β^- : 100 %), including 100 % decay contribution from ^{103}Tc parent ($T_{1/2} = 54.2$ s) are shown in Fig. 17. The TENDL predictions are significantly lower compared to the experiment. The different data sets are in acceptable agreement with each other, in spite of the scattering.

3.1.4.2 $^{nat}\text{Pd}(p,xn)^{97}\text{Ru}$ reaction

The measured experimental cross section data of ^{97}Ru ($I^\pi = 5/2^+$, $T_{1/2} = 2.83$ d, ϵ : 100 %) are cumulative (Fig. 18) including the direct reaction and indirect formation through the ^{97}Ag ($T_{1/2} = 25.5$ s) \rightarrow ^{97}Pd ($T_{1/2} = 3.1$ min) \rightarrow $^{97m,g}\text{Rh}$ ($T_{1/2} = 30.7$ min and 46.2 min) \rightarrow ^{97}Ru decay chain. All measurements agree well, except some single points. Both TENDL versions underestimate the experimental values above 65 MeV.

3.2. Integral yields

The integral yields for $^{103,104m,104g,105g,106m,110m}\text{Ag}$, $^{100,101}\text{Pd}$, $^{99m,100mg,100,101m,101g,102m,102g,105}\text{Rh}$ and $^{97,103}\text{Ru}$ reactions were calculated from spline fits to our experimental excitation functions. The integral yields represent so called physical yields i.e. activity instantaneous production rates (Bonardi, 1987; Otuka and Takács, 2015). The integral yields are shown in Figs. 19 and 20 with experimental thick target yield data found in the literature for the comparison. Only one previous experimental data-set was found in the literature (Hermanne et al., 2004b), which shows good

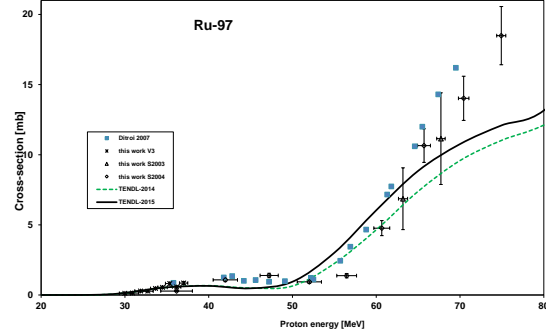


Figure 18: Experimental and theoretical cross sections for proton induced ^{97}Ru (cumulative) production on natural palladium

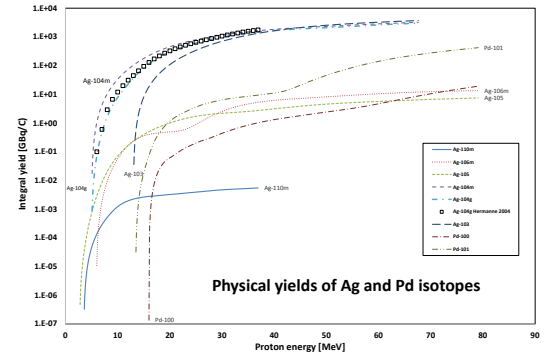


Figure 19: Integral yields for the $^{103,104m,104g,105g,106m,110m}\text{Ag}$ and $^{100,101}\text{Pd}$ producing reactions

agreement with our results (see Fig. 19). On Figs. 19-20 the yield of different isotopes covers a range of 5-6 orders of magnitude, so it is easy to determine, which radio-isotope is economic for production. Out of the production parameters also the radionuclidic purity of the product must be investigated.

4. Overview of production routes of assessed activation products

Many of the investigated radio-products of proton induced nuclear reactions on palladium have applications in different fields of biological studies, nuclear medicine and labeling for industrial processes. Detailed comparison of different production routes would require an ex-

The ^{110m}Ag was used for silver uptake studies in different biological organisms (Zalewska, 2014), for characterization of [^{110m}Ag]-nanoparticles in different organisms, industrial tracing of silver in long term processes, etc. It can be produced via $^{110}\text{Pd}(p,n)$ and $^{110}\text{Pd}(d,2n)$ reaction. In case of deuteron route the ^{111}Ag is produced simultaneously via (d,n) reaction, but it practically does not disturb the above mentioned tracing applications. The $(d,2n)$ requires higher energy cyclotron, the maximum of $(d,2n)$ is shifted above 6 MeV to higher energies.

The ^{105}Rh ($T_{1/2} = 35.36$ h), ^{101m}Rh ($T_{1/2} = 4.34$ d, through ^{101}Pd), ^{101}Rh (3.3 a), ^{97}Ru ($T_{1/2} = 2.83$ d) have been considered as potential candidates for targeted radio-therapeutic use (Pakravan et al., 2015). For production of these radioisotopes the proton induced reactions on palladium play smaller roles. Their production is more advantageous by light charged particle induced reactions on isotopes of ruthenium.

Shortly summarizing: out of the above mentioned radio-products - taking into account different reaction routes - the proton induced reactions on stable isotopes of palladium are more competitive for production of silver isotopes (availability of beams, high cross sections of (p,xn) reactions, etc.).

5. Summary

Excitation functions for direct and cumulative cross-sections for the formation of $^{103,104m,104g,105g,106m,110m}\text{Ag}$, $^{100,101}\text{Pd}$, $^{99m,100,101m,101g,102m,102g}\text{Rh}$ and $^{103,97}\text{Ru}$ radioisotopes on palladium have been measured up to 80 MeV proton energy. Experimental activation cross-section data are presented for the first time in the 70-80 MeV region for all measured isotopes, for ^{104m}Ag , ^{104g}Au , ^{101}Pd , ^{100}Rh and ^{105}Rh in the 40-80 MeV energy range, and for ^{102m}Rh , ^{102g}Rh , ^{101g}Rh , ^{99m}Rh , ^{99g}Rh , ^{103}Ru and ^{97}Ru in the whole energy range. The agreement with the earlier experimental data in the overlapping regions is acceptable good, except one or two cases. The comparison with the theoretical predictions in the TENDL libraries show acceptable agreement, but in several cases, especially by some Ru and Rh (^{103}Ru and $^{102g,101g}\text{Rh}$) radioisotopes, where a continuous feeding from the excited state is possible, systematic underestimation can be observed. Because of the bad statistic by several measurement series large errors and big fluctuations can be observed, especially at higher energy experiments and by low activities, that's why further measurements are encouraged to clarify these cases.

6. Acknowledgements

This work was performed in the frame of the HAS-FWO Vlaanderen (Hungary-Belgium) and HAS-JSPS (Hungary-Japan) projects. The authors acknowledge the support of the research project and of the respective institutions.

References

- Adam-Rebeles, R., Hermanne, A., Van den Winkel, P., De Vis, L., Waegeneer, R., Tarkanyi, F., Takacs, S., Takacs, M. P., 2013. Ge-68/ga-68 production revisited: excitation curves, target preparation and chemical separation - purification. *Radiochimica Acta* 101 (8), 481–489.
- Andersen, H. H., Ziegler, J. F., 1977. Hydrogen stopping powers and ranges in all elements. The stopping and ranges of ions in matter, Volume 3. The Stopping and ranges of ions in matter. Pergamon Press, New York.
- Bakhshabadi, M., Ghorbani, M., Khosroabadi, M., Knaup, C., Meigooni, A. S., 2016. A comparison study on various low energy sources in interstitial prostate brachytherapy. *Journal of Contemporary Brachytherapy* 8 (1), 74–81.
- Batii, V. G., Skakun, E. A., Rakivnenko, Y. N., Rastrepin, O. A., 1988. Absolute and relative cross-sections for (p,n) reactions with production of isomers in silver isotopes. *Soviet Journal of Nuclear Physics-Ussr* 47 (3), 387–390.
- Berglund, M., Wieser, M. E., 2011. Isotopic compositions of the elements. *Pure Appl. Chem.* 83 (2), 397–411.
- BNL, 2015. Bnl isotopes project nuclear data dissemination home page. <http://ie.lbl.gov/toi.html>.
- Bonardi, M., 1987. The contribution to nuclear data for biomedical radioisotope production from the milan cyclotron facility.
- Canberra, 2000. http://www.canberra.com/products/radiochemistry_lab/genie-2000-software.asp.
- Chu, S. Y. F., Ekstr  sm, L. P., Firestone, R. B., 1999. The lund/lbni nuclear data search.
- Dillmann, I., 2006. Determination of proton- and neutron induced cross sections for p-process studies construction of an online database for the p process. Ph.D. thesis, Universitat Basel.
- Dillmann, I., Coquard, L., Domingo-Pardo, C., Kappeler, F., Marganec, J., Uberseder, E., Giesen, U., Heiske, A., Feinberg, G., Hentschel, D., Hilpp, S., Leiste, H., Rauscher, T., Thielemann, F. K., 2011. Cross sections for proton-induced reactions on pd isotopes at energies relevant for the gamma process. *Physical Review C* 84 (1).
- Ditr  i, F., T  rk  nyi, F., Tak  cs, S., Hermanne, A., Ignatyuk, A. V., Baba, M., 2012. Activation cross-sections of deuteron induced reactions on natural palladium. *Nuclear Instruments & Methods in Physics Research Section B-Beam Interactions with Materials and Atoms* 270, 61–74.
- Ditr  i, F., T  rk  nyi, F., Tak  cs, S., Mahunka, I., Csikai, J., Hermanne, A., Uddin, M. S., Hagiwara, M., Baba, M., Ido, T., Shubin, Y., Dityuk, A. I., 2007. Measurement of activation cross sections of the proton induced nuclear reactions on palladium. *Journal of Radioanalytical and Nuclear Chemistry* 272 (2), 231–235.
- Dityuk, A. I., Konobeyev, A. Y., Lunev, V. P., Shubin, Y. N., 1998. New version of the advanced computer code alice-ippe. Tech. rep., IAEA.
- Hermanne, A., Tak  cs, S., T  rk  nyi, F., Bolbos, R., 2004a. Cross section measurements of proton and deuteron induced formation of ag-103 in natural palladium. *Radiochimica Acta* 92 (4-6), 215–218.

- Hermanne, A., Takács, S., Tárkányi, F., Bolbos, R., 2004b. Experimental cross sections for charged particle production of the therapeutic radionuclide ^{111}Ag and its pet imaging analogue $^{104\text{m}}\text{Ag}$. *Nuclear Instruments & Methods in Physics Research Section B-Beam Interactions with Materials and Atoms* 217 (2), 193–201.
- Hermanne, A., Tárkányi, F., Takács, S., Shubin, Y. N., 2005. Experimental determination of cross section of alpha-induced reactions on pd-nat . *Nuclear Instruments & Methods in Physics Research Section B-Beam Interactions with Materials and Atoms* 229 (3–4), 321–332.
- Hu, B. T., Zarubin, P. P., Juravlev, U. U., 1998. Isomeric cross-section ratios resulted from reaction (p,n) on targets ru-100 and pd-104 , pd-106 , pd-110 . *European Physical Journal A* 2 (2), 143–147.
- IAEA-NDS, 2010. Thin layer activation (tla) technique for wear measurement.
- International-Bureau-of-Weights-and-Measures, 1993. Guide to the expression of uncertainty in measurement, 1st Edition. International Organization for Standardization, Geneva, Switzerland.
- Johnson, C. H., Galonsky, A., Kernell, R. L., 1979. (p,n) reaction for $89 < a < 130$ and an anomalous optical-model potential for sub-coulomb protons. *Physical Review C* 20 (6), 2052–2071.
- Khandaker, M. U., Kim, K., Kim, G., Otuka, N., 2010. Cyclotron production of the ^{105}Ag , $^{106\text{m}}\text{Pd}$, ^{100}Pd , ^{101}Rh , ^{100}Rh , $^{101\text{m}}\text{Rh}$, ^{105}Rh radionuclides by $\text{pd-nat}(p,x)$ nuclear processes. *Nuclear Instruments & Methods in Physics Research Section B-Beam Interactions with Materials and Atoms* 268 (14), 2303–2311.
- Kinsey, R. R., Dunford, C. L., Tuli, J. K., Burrows, T. W., 1997. in *Capture Gamma Ray Spectroscopy and Related Topics*, Vol. 2. (NUDAT 2.6 <http://www.nndc.bnl.gov/nudat2/>). Vol. 2. Springer Hungarica Ltd, Budapest.
- Koning, A. J., Rochman, D., 2012. Modern nuclear data evaluation with the talys code system. *Nuclear Data Sheets* 113, 2841.
- Koning, A. J., Rochman, D., Kopecky, J., Sublet, J. C., Bauge, E., Hilaire, S., Romain, P., Morillon, B., Duarte, H., van der Marck, S., Pomp, S., Sjostrand, H., Forrest, R., Henriksson, H., Cabellos, O., S., G., Leppanen, J., Leeb, H., Plompen, A., Mills, R., 2015. Tendl-2015: Talys-based evaluated nuclear data library.
- Koning, A. J., Rochman, D., van der Marck, S., Kopecky, J., Sublet, J. C., Pomp, S., Sjostrand, H., Forrest, R., Bauge, E., Henriksson, H., Cabellos, O., Goriely, S., Leppanen, J., Leeb, H., Plompen, A., Mills, R., 2014. Tendl-2014: Talys-based evaluated nuclear data library.
- Kormali, S. M., Swindle, D. L., Schweikert, E. A., 1976. Charged-particle activation of medium z -elements. 2. proton excitation-functions. *Journal of Radioanalytical Chemistry* 31 (2), 437–450.
- NuDat, 2014. Nudat2 database (2.6).
- Otuka, N., Takács, S., 2015. Definitions of radioisotope thick target yields. *Radiochimica Acta* 103 (1), 1–6.
- Pakravan, D., Ghorbani, M., Meigooni, A. S., 2015. Evaluation of rh-101 as a brachytherapy source. *Journal of Contemporary Brachytherapy* 7 (2), 171–180.
- Pritychenko, B., Sonzogni, A., 2003. Q-value calculator.
- Shubin, Y. N., Lunev, V. P., Konobeyev, A. Y., Dityuk, A. I., 1998. Mendl-2p proton reaction data library for nuclear activation (medium energy nuclear data library). Tech. rep., IAEA.
- Székely, G., 1985. Fgm - a flexible gamma-spectrum analysis program for a small computer. *Computer Physics Communications* 34 (3), 313–324.
- Tárkányi, F., Hermanne, A., Király, B., Takács, S., Ditrói, F., Csikai, J., Fenyvesi, A., Uddin, M. S., Hagiwara, M., Baba, M., Ido, T., Shubin, Y. N., Ignatyuk, A. V., 2009. New cross-sections for production of pd-103 ; review of charged particle production routes. *Applied Radiation and Isotopes* 67 (9), 1574–1581.
- Tárkányi, F., Hermanne, A., Takács, S., Sonck, M., Szűcs, Z., Király, B., Ignatyuk, A. V., 2011. Investigation of alternative production routes of $^{99\text{m}}\text{Tc}$: Deuteron induced reactions on ^{100}Mo . *Appl Radiat Isotopes* 69, 18–25.
- Tárkányi, F., Szelecsényi, F., Takács, S., 1991. Determination of effective bombarding energies and fluxes using improved stacked-foil technique. *Acta Radiologica, Supplementum* 376, 72.
- Zalewska, T., 2014. Bioaccumulation of gamma emitting radionuclides in polysiphonia fucoides. *Journal of Radioanalytical and Nuclear Chemistry* 299 (3), 1489–1497.
- Zarubin, P. P., Sergeev, V. O., 1989. Gamma-ray spectra and production cross-sections of ^{104}Ag isotopes in the reactions $^{104,105,106,108,110}\text{Pd}(p, n\bar{n})$. In: 39th Ann. Conf. Nucl. Spectrosc. Struct. At. Nuclei. p. 1.

Table 3: Decay data of the investigated reaction products ((NuDat, 2014; Pritychenko and Sonzogni, 2003))

Nuclide (isomeric state) Decay path	Half-life	E_{γ} (keV)	I_{γ} (%)	Contributing reaction	Q-value (keV) $gs \rightarrow gs$
^{110m}Ag 117.595 keV IT: 1.33 % β^- : 98.67 %	249.83 d	657.7600 677.6217 706.6760 763.9424 884.6781 937.485 1384.2931 1505.0280	95.61 10.70 16.69 22.60 75.0 35.0 25.1 13.33	$^{110}\text{Pd}(p,n)$	-1656.11
^{106m}Ag 89.667 keV e: 100 %	8.28 d	406.182 429.646 450.976 616.17 717.34 748.36 804.28 824.69 1045.83 1128.02 1199.39 1527.65	13.4 13.2 28.2 21.6 28.9 20.6 12.4 15.3 29.6 11.8 11.2 16.3	$^{106}\text{Pd}(p,n)$ $^{108}\text{Pd}(p,3n)$ $^{110}\text{Pd}(p,5n)$	-3747.49 -19507.09 -34456.89
^{105g}Ag e: 100 %	41.29 d	280.44 331.51 344.52 442.25 443.37 644.55	30.2 4.10 41.4 4.72 10.5 11.1	$^{105}\text{Pd}(p,n)$ $^{106}\text{Pd}(p,2n)$ $^{108}\text{Pd}(p,4n)$ $^{110}\text{Pd}(p,6n)$	-2129.28 -11690.24 -27449.84 -42399.65
^{104m}Ag 6.9022 keV IT: 0.07 % EC: 36.93 % β^+ : 63 %	33.5 min	996.1 1238.8	0.50 3.9	$^{104}\text{Pd}(p,n)$ $^{105}\text{Pd}(p,2n)$ $^{106}\text{Pd}(p,3n)$ $^{108}\text{Pd}(p,5n)$ $^{110}\text{Pd}(p,7n)$	-5061.0 -12155.1 -21716.08 -37475.67 -52425.48
^{104g}Ag EC: 85 % β^+ : 15 %	69.2 min	623.2 863.0 925.9 941.6	2.5 6.9 12.5 25.0	$^{104}\text{Pd}(p,n)$ $^{105}\text{Pd}(p,2n)$ $^{106}\text{Pd}(p,3n)$ $^{108}\text{Pd}(p,5n)$ $^{110}\text{Pd}(p,7n)$	-5061.0 -12155.1 -21716.08 -37475.67 -52425.48
^{103}Ag EC: 73 % β^+ : 27 %	65.7 min	118.74 148.20 266.86 1273.83	31.2 28.3 13.3 9.4	$^{104}\text{Pd}(p,2n)$ $^{105}\text{Pd}(p,3n)$ $^{106}\text{Pd}(p,4n)$ $^{108}\text{Pd}(p,6n)$ $^{110}\text{Pd}(p,8n)$	-13448.35 -20542.46 -30103.43 -45863.02 -45863.02
^{103}Pd e: 100 %	16.991 d	357.45	0.0221	$^{104}\text{Pd}(p,pn)$ $^{105}\text{Pd}(p,p2n)$ $^{106}\text{Pd}(p,p3n)$ $^{108}\text{Pd}(p,p5n)$ $^{110}\text{Pd}(p,p7n)$ ^{103}Ag decay	-9981.26 -17075.36 -26636.34 -42395.93 -57345.72 -13448.35
^{101}Pd EC: 92.8 % β^+ : 7.2 %	8.47 h	269.67 296.29 565.98 590.44	6.43 19 3.44 12.06	$^{102}\text{Pd}(p,pn)$ $^{104}\text{Pd}(p,p3n)$ $^{105}\text{Pd}(p,p4n)$ $^{106}\text{Pd}(p,p5n)$ $^{108}\text{Pd}(p,p7n)$ $^{110}\text{Pd}(p,p9n)$ ^{101}Ag decay	-10571.66 -28178.28 -35272.38 -44833.35 -60592.94 -75542.72 -15450.29
^{100}Pd e: 100 %	3.63 d	74.78 84.00 126.15 158.87	48 52 7.8 1.66	$^{102}\text{Pd}(p,p2n)$ $^{104}\text{Pd}(p,p4n)$ $^{105}\text{Pd}(p,p5n)$ $^{106}\text{Pd}(p,p6n)$ $^{108}\text{Pd}(p,p8n)$ $^{110}\text{Pd}(p,p10n)$ ^{100}Ag decay	-18846.41 -36453.02 -43547.11 -53108.14 -68867.76 -26718.02
^{105}Rh β^- : 100 %	35.36 h	306.1 318.9	5.1 19.1	$^{106}\text{Pd}(p,2p)$ $^{108}\text{Pd}(p,2p2n)$ $^{110}\text{Pd}(p,2p4n)$	-9345.82 -25105.42 -40055.23
^{102m}Rh 140.7 keV IT: 0.23 % e: 99.77 %	3.742 a	631.29 697.49 766.84 1046.59 1112.84	56.0 44.0 34.0 34.0 19.0	$^{104}\text{Pd}(p,2pn)$ $^{105}\text{Pd}(p,2p2n)$ $^{106}\text{Pd}(p,2p3n)$ $^{108}\text{Pd}(p,2p5n)$ $^{110}\text{Pd}(p,2p7n)$	-17974.84 -25068.94 -34629.91 -50389.49 -65339.29
^{102g}Rh β^- : 22 % EC: 78 %	207.3 d	468.58 739.5 1158.10	2.9 0.53 0.58	$^{104}\text{Pd}(p,2pn)$ $^{105}\text{Pd}(p,2p2n)$ $^{106}\text{Pd}(p,2p3n)$ $^{108}\text{Pd}(p,2p5n)$ $^{110}\text{Pd}(p,2p7n)$	-17974.84 -25068.94 -34629.91 -50389.49 -65339.29
^{101m}Rh 157.32 keV IT: 7.20% EC: 92.8%	4.34 d	306.857 545.117	81 4.3	$^{102}\text{Pd}(p,2p)$ $^{104}\text{Pd}(p,2p2n)$ $^{105}\text{Pd}(p,2p3n)$ $^{106}\text{Pd}(p,2p4n)$ $^{108}\text{Pd}(p,2p6n)$ $^{110}\text{Pd}(p,2p8n)$ ^{101}Pd decay	-7809.14 -25415.76 -32509.86 -42070.83 -57830.41 -72780.20 -10571.66
^{101g}Rh e: 100 %	3.3 a	127.226 198.01 325.23	68 73 11.8	$^{102}\text{Pd}(p,2p)$ $^{104}\text{Pd}(p,2p2n)$ $^{105}\text{Pd}(p,2p3n)$ $^{106}\text{Pd}(p,2p4n)$ $^{108}\text{Pd}(p,2p6n)$ $^{110}\text{Pd}(p,2p8n)$ ^{101}Pd decay	-7809.14 -25415.76 -32509.86 -42070.83 -57830.41 -72780.20 -10571.66
^{100}Rh EC: 96.1 % β^+ : 3.9 %	20.8 h	446.153 539.512 822.654 1107.223 1553.348	11.98 80.6 21.09 13.57 20.67	$^{102}\text{Pd}(p,2pn)$ $^{104}\text{Pd}(p,2p3n)$ $^{105}\text{Pd}(p,2p4n)$ $^{106}\text{Pd}(p,2p5n)$ $^{108}\text{Pd}(p,2p7n)$ $^{110}\text{Pd}(p,2p9n)$	-17703.1 -35309.7 -42403.8 -51964.7 -67724.3 -

Table 3: continued

Nuclide (isomeric state) Decay path	Half-life	E_γ (keV)	I_γ (%)	Contributing reaction	Q-value (keV) gs \rightarrow gs
^{99m} Rh 64.3 keV ϵ : >99.84 % IT:<0.16 %	4.7 h	340.8 617.8 1261.2	69 11.8 10.9	¹⁰² Pd(p,2p2n) ¹⁰⁴ Pd(p,2p4n) ¹⁰⁵ Pd(p,2p5n) ¹⁰⁶ Pd(p,2p6n) ¹⁰⁸ Pd(p,2p8n) - ¹¹⁰ Pd(p,2p10n) ⁹⁹ Pd decay	-25784.61 -43391.23 -50485.34 -60046.29 -75805.87 - -29963.71
^{99g} Rh EC: 96.4 % β^+ : 3.6 %	16.1 d	89.76 353.05 528.24	33.4 34.6 38.0	¹⁰² Pd(p,2p2n) ¹⁰⁴ Pd(p,2p4n) ¹⁰⁵ Pd(p,2p5n) ¹⁰⁶ Pd(p,2p6n) ¹⁰⁸ Pd(p,2p8n) - ¹¹⁰ Pd(p,2p10n)	-25784.61 -43391.23 -50485.34 -60046.29 -75805.87 - -
¹⁰³ Ru β^- : 100 %	39.247 d	497.085	91.0	¹⁰⁵ Pd(p,3p) ¹⁰⁶ Pd(p,3pn) ¹⁰⁸ Pd(p,3p3n) ¹¹⁰ Pd(p,3p5n) ¹⁰³ Tc decay	-15732.06 -25293.02 -41052.62 -56002.41 -27172.42
⁹⁷ Ru ϵ : 100 %	2.83 d	215.70 324.49	85.62 10.79	¹⁰² Pd(p,3p3n) ¹⁰⁴ Pd(p,3p5n) ¹⁰⁵ Pd(p,3p6n) ¹⁰⁶ Pd(p,3p7n) ⁹⁷ Rh decay	-40603.59 -58210.2 -65304.29 -74865.26 -50481.75

Increase the Q-values if compound particles are emitted by: np-d, +2.2 MeV; 2np-t, +8.48 MeV; n2p-³He, +7.72 MeV; 2n2p- α , +28.30 MeV. Decrease Q-values for isomeric states with level energy of the isomer

Table 4: Experimental cross sections of $^{nat}\text{Pd}(\text{p},\text{xn})^{103,104m,104g,105g,106m,110m}\text{Ag}$, $^{100,101}\text{Pd}$ and ^{97}Ru reactions

E±ΔE (MeV)		Exp.	^{110m} Ag		^{106m} Ag		¹⁰⁵ Ag		^{104m} Ag		^{104g} Ag		¹⁰³ Ag		¹⁰¹ Pd		¹⁰⁰ Pd		⁹⁷ Ru	
15.8	0.5	V1	1.81	0.32					85.53	18.69					1.41	0.17				
14.9	0.5								79.70	10.40					0.55	0.08				
14.0	0.5			3.32	0.42				62.07	8.10										
13.0	0.6			4.43	0.59				43.02	5.27										
11.9	0.6			5.84	0.70				34.48	6.09										
10.8	0.6			7.06	0.82				29.99	4.92										
9.5	0.7			8.91	1.02				32.51	4.15										
8.2	0.8			6.46	0.75				17.40	2.57										
6.7	0.9							7.78	2.20											
28.2	0.5	V2	1.66	0.31											6.48	0.84	4.75	0.54		
26.6	0.5			1.68	0.30				61.76	12.87					7.78	1.01	7.55	0.85		
25.0	0.5			1.67	0.29				68.69	10.80					9.79	1.20	8.42	0.95		
23.7	0.6			1.67	0.26									5.46	0.76	3.59	0.41			
22.4	0.6								65.96	9.19				5.84	0.66	6.65	0.77			
21.1	0.7		1.30	0.23					75.79	9.90				6.79	0.77	5.17	0.58			
19.7	0.8								66.73	8.47				6.88	0.86	3.14	0.36			
18.2	0.9		1.55	0.20					83.95	10.23				5.26	0.66	0.21	0.06			
16.5	1.0		1.48	0.20					80.87	10.60				3.15	0.44					
15.9	0.8								76.81	9.03										
37.0	0.5	V3	1.07	0.31											7.69	1.51	15.58	2.15	0.85	0.10
36.2	0.5														4.45	0.52	7.62	1.35	0.57	0.07
35.4	0.5														5.41	0.64	11.80	1.06	0.81	0.10
34.5	0.5														4.41	0.51	8.78	1.50	0.55	0.07
33.6	0.6														5.09	0.59	11.64	1.02	0.46	0.06
32.7	0.6														4.75	0.55	9.36	1.73	0.28	0.04
31.9	0.7														5.32	0.61	10.29	0.94	0.28	0.04
30.9	0.7														6.18	0.71	7.22	1.37	0.14	0.03
30.0	0.8		1.22	0.31										6.91	0.79	11.44	1.66	0.12	0.03	
29.0	0.7													7.53	0.86	8.33	1.82			
28.0	0.5													8.07	0.92	7.62	0.77			
27.0	0.6													7.13	0.84	1.69	0.61			
25.9	0.7		1.39	0.31										9.55	1.09	7.05	0.65			
24.8	0.8		1.53	0.20										8.40	0.95	3.04	0.66			
23.7	1.0		1.05	0.25										9.15	1.04	6.71	1.10			
22.5	1.1		1.58	0.19										9.22	1.05	2.69	0.55			
21.4	1.3		1.58	0.19										8.85	1.00	4.94	0.43			
20.1	1.4		1.50	0.18										7.58	0.86	1.65	0.32			
79.2	0.5	S2004			18.68	2.11	66.67	7.52							108.60	12.25	67.17	11.27	25.83	2.90
74.9	0.5				17.29	1.95	62.51	7.05							93.93	10.58	68.45	11.06	18.49	2.08
70.4	0.6				21.78	2.46	71.52	8.07							114.58	12.91	52.54	9.56	14.02	1.58
65.7	0.8				32.70	3.69	90.62	10.21							112.34	12.66	51.60	11.17	10.65	1.20
60.7	1.0				41.61	4.68	100.38	11.30							101.66	11.42	39.92	9.92	4.77	0.54
56.5	1.2				42.67	4.80	98.39	11.08							79.06	8.92	18.38	4.63	1.38	0.16
52.0	1.4				43.72	4.92	144.36	16.22							61.28	6.92	11.39	4.61	0.93	0.11
47.2	1.1				41.22	4.64	196.98	22.13							40.52	4.59	12.25	2.04	1.39	0.16
42.0	1.5			71.81	8.07	163.15	18.34							10.45	1.26	9.34	1.12	1.08	0.12	
36.2	1.9			125.50	14.10	89.97	10.13							7.23	0.89	6.02	1.00	0.29	0.04	
67.7	0.5	S2003							27.38	4.44	46.48	5.36	56.5	6.8	84.56	11.00	47.57	2.38	11.15	3.27
63.2	0.5									19.92	3.36	51.15	5.78	59	6.8	82.24	10.07		6.86	2.20
58.4	0.6									31.83	5.89	68.05	7.81	56.3	6.7	90.87	10.91			
53.2	0.8									32.31	5.01	55.70	6.41	77.7	8.7	65.31	8.44			
47.6	1.0								22.45	4.07	41.71	4.84	96	10	38.20	5.61				
41.3	1.2								41.56	6.47	75.73	8.68	123	12	9.88	4.14				
34.1	1.6								55.62	8.45	110.26	12.56	149	13						
69.5	0.5	S2002-1													96.65	10.92				
65.5	0.5														93.07	10.45				
61.3	0.6														91.33	10.23				
56.9	0.7														82.07	9.37				
52.2	0.9													67.61	7.71					
47.2	1.1													46.46	5.52					
41.8	1.4													24.67	3.38					
35.8	1.8													5.39	1.89					
28.9	2.2													7.72	2.19					
67.4	0.5	S2002-2													101.94	11.09				
64.6	0.5														97.10	10.59				
61.8	0.6														95.12	10.39				
58.8	0.7														92.19	10.07				
55.7	0.8														85.91	9.40				
52.5	0.9														71.21	7.81				
49.1	1.1														56.71	6.26				
45.6	1.3														41.65	4.63				
44.2	1.6													34.74	3.88					
42.8	1.8													27.61	3.01					

Table 5: Experimental cross sections of $^{nat}\text{Pd}(\text{p},\text{xn})^{99\text{m},99\text{g},100,101\text{m},101\text{g},102\text{m},102\text{g},105}\text{Rh}$ and ^{103}Ru reactions

E±ΔE (MeV)		Exp.	σ ± Δσ (mb)																	
			105Rh		102mRh		102gRh		101mRh		101gRh		100Rh		99mRh		99gRh		103Ru	
15.8	0.5	V1	4.53	0.51					3.14	0.35	4.25	1.02								
14.9	0.5		4.40	0.50					1.87	0.21										
14.0	0.5		3.92	0.45					1.00	0.12										
13.0	0.6		3.42	0.39					0.68	0.08										
11.9	0.6		2.65	0.31					0.53	0.07										
10.8	0.6		2.04	0.24					0.28	0.04										
9.5	0.7		1.74	0.20					0.25	0.03										
8.2	0.8		1.05	0.13					0.11	0.02										
6.7	0.9		0.54	0.06					0.03	0.01										
28.2	0.5	V2	3.80	0.44					18.30	2.06	6.77	0.98	8.81	0.99						
26.6	0.5		4.62	0.54					19.65	2.21	5.12	0.85	6.64	0.75						
25.0	0.5		5.41	0.62					18.60	2.09			4.91	0.55						
23.7	0.6		6.39	0.73					18.53	2.08	3.40	0.62	4.04	0.46						
22.4	0.6		6.00	0.68					16.56	1.86			1.19	0.13						
21.1	0.7		7.09	0.81					17.10	1.92			2.01	0.23						
19.7	0.8		7.30	0.83					13.81	1.55			0.89	0.11						
18.2	0.9		6.85	0.78					10.51	1.18			0.19	0.03						
16.5	1.0		6.55	0.74					5.89	0.66										
15.9	0.8		5.91	0.67					4.25	0.48										
37.0	0.5	V3	5.53	0.64		11.31	1.43	22.65	2.55	6.95	1.42	20.10	2.28	5.95	0.69	2.42	0.30			
36.2	0.5		4.66	0.53		13.26	1.61	17.05	1.92	6.84	1.37	15.42	1.74	4.43	0.51	1.59	0.21			
35.4	0.5		5.92	0.68				21.53	2.42	8.44	1.65	20.82	2.36	5.17	0.61	2.15	0.27			
34.5	0.5		4.98	0.57				18.38	2.06	6.81	1.47	17.68	2.00	3.93	0.46	1.92	0.25			
33.6	0.6		4.65	0.54				18.86	2.12	5.93	1.42	17.17	1.95	3.89	0.46	1.26	0.19			
32.7	0.6		4.00	0.47				16.71	1.88	7.88	1.53	14.84	1.68	2.73	0.32	1.04	0.17			
31.9	0.7		4.12	0.47				18.51	2.08			15.04	1.70	2.14	0.27	0.78	0.15			
30.9	0.7		4.06	0.47				19.50	2.19			14.07	1.59	1.77	0.23	0.35	0.11			
30.0	0.8		3.96	0.47				19.09	2.15			11.87	1.35	0.90	0.14					
29.0	0.7		3.57	0.42				18.97	2.13			9.62	1.10	0.60	0.10					
28.0	0.5		3.41	0.40				18.71	2.10			7.62	0.88	0.35	0.10					
27.0	0.6		3.54	0.42				16.55	1.86			5.64	0.66							
25.9	0.7		4.28	0.50				19.86	2.23			5.80	0.67							
24.8	0.8		4.31	0.49				16.53	1.86			4.21	0.48							
23.7	1.0		4.94	0.57				16.88	1.90			3.68	0.43							
22.5	1.1		5.60	0.64				16.72	1.88			3.38	0.40							
21.4	1.3		5.78	0.65				15.63	1.76			2.00	2.01							
20.1	1.4		5.68	0.64				13.40	1.51			0.92	0.12							
79.2	0.5	S2004	12.58	1.80	31.20	10.35	23.46	3.26	182.86	20.53	15.39	6.23	55.22	6.20	37.20	4.19	7.28	0.88	1.37	0.25
74.9	0.5		11.81	1.37	26.58	8.92	18.78	2.53	156.44	17.56	21.38	5.74	41.37	4.65	25.87	2.91	5.71	0.70	1.19	0.22
70.4	0.6		10.90	1.30	22.82	10.73	19.82	2.88	158.23	17.76	11.40	3.72	43.88	4.93	27.04	3.05	5.35	0.65	0.86	0.17
65.7	0.8		8.82	1.05	23.78	13.09	26.39	3.43	184.09	20.67			34.51	3.88	24.72	2.79	6.33	0.77	1.13	0.22
60.7	1.0		10.20	1.17	24.51	7.54	31.09	3.98	168.28	18.89			27.99	3.14	23.83	2.68	6.38	0.76	0.87	0.19
56.5	1.2		7.27	0.88	19.53	7.09	27.96	3.57	123.82	13.90	6.97	3.70	24.05	2.70	20.24	2.28	5.13	0.61	0.65	0.17
52.0	1.4		6.23	0.78	14.98	9.42	27.73	3.41	95.23	10.69	8.63	4.54	23.62	2.65	19.43	2.19	5.07	0.59	0.61	0.13
47.2	1.1		7.65	0.88	7.44	1.79	23.51	2.99	67.12	7.54			22.32	2.51	15.66	1.77	4.20	0.50	0.51	0.14
42.0	1.5		6.71	0.78	5.06	1.46			29.10	3.27	8.16	4.91	19.62	2.21	6.94	0.79	2.62	0.37	0.34	0.16
36.2	1.9		3.94	0.44					21.61	2.43			13.62	1.53	2.27	0.28	0.63	0.22		
67.7	0.5	S2003											30.10	9.79			4.67	1.41		
63.2	0.5												23.34	3.42						
58.4	0.6												22.15	3.18						
53.2	0.8												23.34	3.62						
47.6	1.0												20.46	3.13						
41.3	1.2												17.57	2.97						
34.1	1.6												10.19	2.55						
69.5	0.5	S2002-1	16.34	2.93	20.48	9.18	26.83	4.92					47.96	5.24	22.79	3.74	6.99	0.78		
65.5	0.5		15.20	2.79	12.25	7.61	26.83	4.89					39.57	4.33	20.49	3.36	6.58	0.93	1.16	0.35
61.3	0.6		9.92	2.08	15.03	8.84	23.53	4.48					32.47	3.56	18.41	3.19	5.15	0.75	0.67	0.39
56.9	0.7		12.03	2.52	17.96	9.30	23.10	4.37					27.92	3.08	20.37	3.62	4.27	0.66		
52.2	0.9		10.48	2.06	16.79	8.79	22.46	4.39					26.00	2.86	20.06	3.28	4.58	0.65		
47.2	1.1		10.58	1.97	13.56	8.80	22.25	4.36					23.04	2.54	19.71	3.23	3.18	0.60		
41.8	1.4		9.27	2.04	8.25	8.05	12.92	2.98					20.40	2.26	9.66	2.42	1.80	0.57		
35.8	1.8		7.83	2.12			10.73	2.83					18.03	2.02	6.46	2.56				
28.9	2.2		3.83	1.64									8.35	0.98						
67.4	0.5	S2002-2	12.18	3.47	15.10	2.53	27.65	2.03					33.91	3.69	23.38	2.56	4.31	0.76	1.30	0.39
64.6	0.5		13.75	3.93	14.65	2.64	24.61	1.81					29.13	3.19	21.36	2.35	4.94	0.84	0.75	0.44
61.8	0.6		10.34	3.20	16.61	2.91	27.13	1.98					26.30	2.88	20.16	2.23	5.28	0.92		
58.8	0.7		11.34	3.36	14.10	2.97	23.52	1.75					24.63	2.70	19.85	2.20	4.46	0.68		
55.7	0.8		8.11	3.31	15.70	2.83	22.81	1.71					24.33	2.67	20.26	2.24	5.50	0.82		
52.5	0.9		8.48	3.12	13.98	2.71	22.15	1.65					23.91	2.63	18.47	2.05	4.71	0.71		
49.1	1.1		8.00	3.01	12.02	2.38	19.81	1.58					22.60	2.48	17.06	1.90	3.84	0.66		
45.6	1.3		4.12	2.84	6.14	2.29	16.92	1.34					21.16	2.33	14.99	1.68	3.15	0.63		
44.2	1.6		5.45	2.75	8.86	2.84	13.55	1.19					20.48	2.26	13.78	1.56	2.89	0.53		
42.8	1.8		4.78	1.45	5.75	2.20	11.61	1.08					19.50	2.12	11.61	1.27	2.67	0.31		